

Interplay of 95 GeV Diphoton Excess and Dark Matter in Supersymmetric Triplet Model

Zetian Li,¹ Ning Liu,^{2,*} and Bin Zhu^{1,†}

¹*Department of Physics, Yantai University, Yantai 264005, China*

²*Department of Physics and Institute of Theoretical Physics, Nanjing Normal University, Nanjing, 210023, China*

The decay of the Higgs boson and the nature of dark matter remain fundamental challenges in particle physics. We investigate the 95 GeV diphoton excess and dark matter within the framework of the triplet-extended Minimal Supersymmetric Standard Model (TMSSM). In this model, an additional Hypercharge $Y = 0$, $SU(2)_L$ triplet superfield is introduced. Mixing between the triplet and doublet Higgs states enhances the diphoton signal strength of the 95 GeV Higgs boson, resulting in $\mu_{\gamma\gamma}^{\text{CMS+ATLAS}} = 0.24^{+0.09}_{-0.08}$, which is consistent with experimental observations. This enhancement arises primarily from charged Higgs and chargino loop contributions. Additionally, the model accommodates viable dark matter candidates in the form of a bino-dominated neutralino. The relic density is reduced to the observed value through resonance-enhanced annihilation via the Higgs portal or co-annihilation with the triplino or higgsino. This reduction remains consistent with constraints from direct and indirect detection experiments. A comprehensive parameter scan demonstrates that the TMSSM can simultaneously explain the 95 GeV diphoton excess, the observed 125 GeV Higgs mass, and the dark matter relic density, establishing a compelling and theoretically consistent framework.

I. INTRODUCTION

The Standard Model (SM) of particle physics, a cornerstone of our understanding of fundamental interactions, faces significant challenges in explaining the hierarchy problem of Higgs boson mass and the nature of dark matter (DM). The SM cannot stabilize the Higgs mass against quantum corrections, a deficiency known as the hierarchy problem [1, 2], which results in sensitivity to ultraviolet (UV) divergences. Supersymmetry [3, 4] offers a compelling solution by introducing supersymmetric partners that cancel quadratic loop corrections, thereby stabilizing the Higgs mass and reducing fine-tuning. The lightest supersymmetric particle (LSP), stabilized by R-parity, serves as a natural DM candidate, often identified as the neutralino [5, 6].

The Minimal Supersymmetric Standard Model (MSSM) addresses both the hierarchy problem and DM, but the lack of experimental evidence for superpartners has led to the "little hierarchy problem" [7–10]. This problem arises from the difficulty in reconciling the observed 125 GeV Higgs boson mass with the non-observation of stops and gluinos [11, 12]. The Triplet-Extended MSSM (TMSSM) [13–26] potentially resolves this challenge by introducing an $SU(2)_L$ triplet superfield. This addition enhances quartic couplings, providing a natural solution to the little hierarchy problem [27].

Recent data from CMS [28, 29] and ATLAS [30, 31] report a significant signal for a 95 GeV Higgs boson decaying to diphotons. CMS observes a local excess with 2.9σ significance and a signal strength of $\mu_{\gamma\gamma} = 0.33^{+0.19}_{-0.12}$, while ATLAS finds $\mu_{\gamma\gamma} = 0.18 \pm 0.10$. The combined signal strength, $\mu_{\gamma\gamma}^{\text{CMS+ATLAS}} = 0.24^{+0.09}_{-0.08}$ [32], suggests the 95 GeV Higgs may exceed the SM prediction, indicating potential new physics.

Triplet-extended models introduce an $SU(2)_L$ triplet scalar field, which can explain the 95 GeV diphoton excess through

mixing with the SM Higgs doublet, enhancing the diphoton decay rate. This mechanism has been extensively studied in non-supersymmetric frameworks [32–66], where precise tuning of triplet-doublet mixing and mass splittings between charged and neutral Higgs states amplifies the diphoton signal strength while satisfying experimental constraints. In supersymmetry, the singlet-extended MSSM has also been thoroughly investigated [67–73]. Given this promising property, it is compelling to explore whether the TMSSM, the supersymmetric generalization, retains this feature. In the TMSSM, supersymmetry imposes strict relations on coupling constants, avoiding the artificial adjustments often required in non-supersymmetric models. This rigidity may preserve the enhanced diphoton signal necessary to explain the 95 GeV excess while eliminating the need for fine-tuning couplings, offering a significant advantage over non-supersymmetric approaches.

Additionally, the triplet Higgs field introduces new annihilation channels for neutralinos [24], especially when the triplet mass is approximately twice the neutralino mass, around 95 GeV or 125 GeV. The triplino, the supersymmetric partner of the triplet Higgs, plays a crucial role in neutralino annihilation. We demonstrate that even if the triplino is not the LSP, it can significantly influence DM annihilation by modifying chargino masses. This modification substantially alters the DM relic density through bino-triplino co-annihilation processes [74].

In this work, we show that the TMSSM simultaneously accounts for the 95 GeV diphoton excess and dark matter phenomenology. Through a detailed analysis of the Higgs and neutralino sectors and a comprehensive parameter scan, we identify viable parameter regions that satisfy all relevant constraints, presenting a compelling extension of the SM.

This paper is structured as follows: Section II presents the TMSSM framework, focusing on the impact of the $SU(2)_L$ triplet superfield on the Higgs sector. We analytically demonstrate how the triplet accounts for the 95 GeV Higgs and its diphoton excess. Section III explores the roles of the triplet and triplino in dark matter phenomenology, analyzing their effects on annihilation cross-sections and relic density while

* liuning@njnu.edu.cn

† zhubin@mail.nankai.edu.cn

ensuring consistency with detection constraints. Section IV evaluates the TMSSM's ability to simultaneously address the Higgs decay and dark matter problems through a comprehensive parameter scan. Section V summarizes the findings and discusses their broader implications for physics beyond the Standard Model.

II. HIGGS SECTOR: HIGGS MASS AND ITS DECAY

The TMSSM extends the MSSM through the introduction of an additional $SU(2)_L$ -triplet superfield Σ ,

$$\Sigma = \begin{pmatrix} T^0/\sqrt{2} & T^+ \\ T^- & -T^0/\sqrt{2} \end{pmatrix}. \quad (1)$$

The TMSSM superpotential adds two terms: a triplino mass term μ_T and a cubic coupling λ that mixes the triplet with the Higgs doublets. The full superpotential reads,

$$W_{\text{TMSSM}} = W_{\text{MSSM}} + \lambda H_u \cdot \Sigma H_d + \mu_T \text{Tr } \Sigma^2. \quad (2)$$

The model also incorporates soft SUSY-breaking terms:

$$\mathcal{L}_{\text{soft}} = \mathcal{L}_{\text{MSSM}_S} + m_T^2 \text{Tr}(\Sigma^\dagger \Sigma) + B_{\mu_T} \text{Tr}(\Sigma^2) + T_\lambda H_u \cdot \Sigma H_d + \text{h.c.}, \quad (3)$$

where only triplet-specific terms are explicitly listed. To simplify the analysis, we choose a SUSY-breaking scale M_S to unify the soft masses $M_S = m_{\tilde{Q}} = m_{\tilde{u}} = m_{\tilde{d}} = m_{\tilde{L}} = m_{\tilde{e}}$, and A_0 to represent the trilinear soft terms $A_0 = A_u = A_d = A_e$. The remaining soft masses $m_{H_u}^2$, $m_{H_d}^2$, and m_T^2 are determined by imposing the conditions for successful electroweak symmetry breaking (EWSB), i.e., the tadpole equations $\partial V / \partial \phi_i = 0$, where i corresponds to H_u , H_d , and T .

During the EWSB process, the neutral component T^0 of the triplet acquires a vacuum expectation value (VEV). The neutral components of the Higgs doublets and the triplet can be expressed as fluctuations around their respective VEVs:

$$\begin{aligned} H_d^0 &= \frac{1}{\sqrt{2}} (v_d + \phi_d + i\sigma_d), \\ H_u^0 &= \frac{1}{\sqrt{2}} (v_u + \phi_u + i\sigma_u), \\ T^0 &= \frac{1}{\sqrt{2}} (v_T + \phi_T + i\sigma_T), \end{aligned} \quad (4)$$

where v_d , v_u , and v_T are the VEVs of the Higgs doublets and the triplet, respectively. The terms ϕ_d , ϕ_u , and ϕ_T represent their real parts, while σ_d , σ_u , and σ_T denote their imaginary parts.

The electroweak scale is defined by the Higgs vacuum expectation values (VEVs) as $v = \sqrt{v_d^2 + v_u^2} = 246$ GeV. Triplet-extended models face constraints from electroweak precision tests (EWPT), particularly through the ρ parameter. A non-zero triplet VEV v_T alters ρ from unity according to $\rho = 1 + \frac{4v_T^2}{v^2}$. With the experimental value $\rho = 1.0004^{+0.0003}_{-0.0004}$, this limits $v_T \lesssim 4$ GeV. However, introducing two additional

triplet chiral superfields with hypercharges $Y = \pm 1$, alongside the $Y = 0$ triplet, preserves custodial symmetry in the superpotential [75]. This ensures $\rho = 1$ at tree level, permitting a larger triplet VEV v_T while remaining consistent with EWPT constraints.

Due to the mixing between different gauge eigenstates, (ϕ_d, ϕ_u, ϕ_T) , they form the non-diagonal CP-even Higgs mass matrix.

$$\mathcal{M}_h^2 = \begin{pmatrix} \mathcal{M}_{\phi_d \phi_d} & \mathcal{M}_{\phi_u \phi_d} & \mathcal{M}_{\phi_T \phi_d} \\ \mathcal{M}_{\phi_d \phi_u} & \mathcal{M}_{\phi_u \phi_u} & \mathcal{M}_{\phi_T \phi_u} \\ \mathcal{M}_{\phi_d \phi_T} & \mathcal{M}_{\phi_u \phi_T} & \mathcal{M}_{\phi_T \phi_T} \end{pmatrix}. \quad (5)$$

In the limit of small v_T and λ , the triplet sector almost decouples from the doublet sector. Consequently, the 95 GeV Higgs predominantly originates from the triplet itself. We therefore analyze the (33)-th component of the mass matrix first and denote the lightest higgs mass by m_h ,

$$m_h^2 = \mathcal{M}_{\phi_T \phi_T} = 2B_{\mu_T} + 4\mu_T^2 + m_T^2, \quad (6)$$

where m_T^2 can be determined by solving the tadpole equations at the EWSB scale $\partial V / \partial \phi_T = 0$,

$$\begin{aligned} m_T^2 = -2B_{\mu_T} - 4\mu_T^2 &+ \frac{\lambda}{2} \left(\frac{v}{v_T} \right) v \mu_T \sin(2\beta) \\ &- \frac{\lambda}{4} \left(\frac{v}{v_T} \right) v \mu \sin^2 \beta, \end{aligned} \quad (7)$$

This relation holds exclusively at tree-level, neglecting terms linear in λ and v_T . We note, however, that a linear term in λ persists in Eq. (7) due to the v/v_T enhancement, which counteracts the λ suppression. Substituting m_T^2 from Eq. (7) into the triplet Higgs mass (Eq. (6)), we observe a precise cancellation of B_{μ_T} ,

$$m_h^2 = \frac{\lambda}{2} \left(\frac{v}{v_T} \right) v \mu_T \sin(2\beta) - \frac{\lambda}{4} \left(\frac{v}{v_T} \right) v \mu \sin^2 \beta. \quad (8)$$

This cancellation explains the independence of the lightest Higgs boson mass on B_{μ_T} in Fig. 1 (left panel). The residual minor dependence on B_{μ_T} arises from loop-level corrections.

The right panel of Fig. 1 shows that the mass of the triplet-dominated lightest Higgs is inversely proportional to μ_T , which appears to contradict the linear dependence on μ_T predicted by Eq. (8). This apparent contradiction is resolved by the negative cubic coupling λ , which reverses the proportionality. Consequently, the lightest Higgs mass scales inversely with μ_T , as depicted in Fig. 1. We numerically exclude the light-gray region where the squared mass of the charged Higgs, $m_{H^\pm}^2$, is negative.

The doublet Higgs is responsible for the observed 125 GeV Higgs boson. The tree-level Higgs mass enhancement, proportional to $\lambda^2 v^2 \sin^2 2\beta$, is suppressed due to the small value of λ . Therefore, we rely on a high supersymmetry (SUSY)

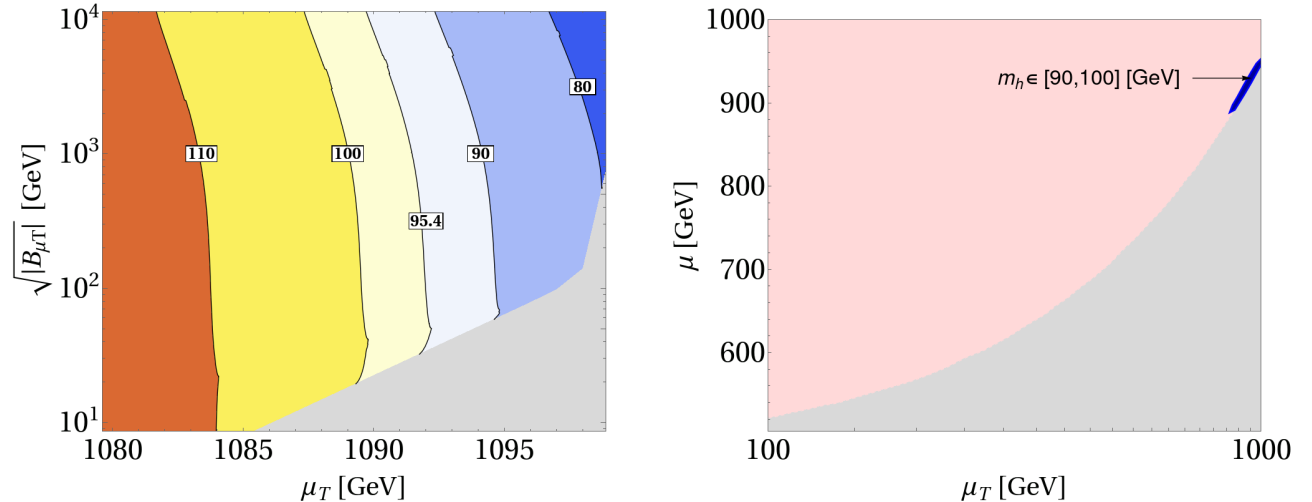


Figure 1. Left: Contour plot of the lightest Higgs mass m_h in the $\sqrt{B_{\mu_T}} - \mu_T$ parameter space, with $\mu = 1$ TeV, $M_S = 5.01$ TeV, $A_0 = 12$ TeV. Right: Contour plot of the lightest Higgs boson mass m_h in the $\mu - \mu_T$ parameter space, with $M_S = 5.01$ TeV, $A_0 = 12$ TeV, and $\sqrt{B_{\mu_T}} = \sqrt{5}$ TeV.

scale and large trilinear couplings to achieve the required Higgs mass. The left panel of Fig. 2 illustrates that maximal mixing ($A_0 \sim M_S$) greatly enhances the Higgs mass, avoiding the need for very large M_S values. When A_0 is small, the Higgs mass depends more on the SUSY scale M_S , requiring larger M_S for higher Higgs boson masses.

The right panel of Fig. 2 reveals that the triplet parameter μ_T influences the SM Higgs boson mass, despite the nominal decoupling of the triplet sector. Direct inspection shows that the $\mathcal{M}_{\phi_d \phi_d}$ and $\mathcal{M}_{\phi_u \phi_u}$ mass matrix components depend on μ_T through the highly suppressed term $\lambda v_T/v$, allowing these contributions to be safely neglected. The μ_T dependence instead arises from the off-diagonal mixing terms $\mathcal{M}_{\phi_u \phi_T}$ and $\mathcal{M}_{\phi_d \phi_T}$. For example, the $\mathcal{M}_{\phi_u \phi_T}$ component is

$$\mathcal{M}_{\phi_u \phi_T} = -\lambda v(\mu_T \cos \beta - \mu \sin \beta) + \mathcal{O}(\lambda^2). \quad (9)$$

Despite $\lambda \sim \mathcal{O}(-0.1)$, its residual contribution induces a measurable shift in the 95 and 125 GeV Higgs boson mass. The mixing between the doublet and triplet Higgs fields $h = \phi_{SM} \cos \theta + \phi_T \sin \theta$ is essential for the production of the lightest neutral Higgs boson via gluon fusion. Without this mixing, gluon fusion—the dominant production mechanism—would be absent, as the triplet Higgs does not couple directly to fermions.

Alternative processes, such as vector boson fusion or associated production, typically yield insufficient cross-sections.

Thus, doublet-triplet mixing is necessary to achieve a sufficiently large production cross-section via gluon fusion, explaining the observed diphoton excess, which is determined as follows,

$$\mu_{\gamma\gamma} = \frac{\sigma_{SUSY}(pp \rightarrow h) \times Br_{SUSY}(h \rightarrow \gamma\gamma)}{\sigma_{SM}(pp \rightarrow h) \times Br_{SM}(h \rightarrow \gamma\gamma)}. \quad (10)$$

To influence $\mu_{\gamma\gamma}$, modifications to either the Higgs production mechanism or its decay width are required. Owing to the small doublet-triplet mixing angle θ , the gluon fusion production cross-section remains significant, analogous to the SM mechanism. The gluon fusion cross-section for h is,

$$\sigma_{ggF} \propto |\cos \theta \cdot A_t(\tau_t) + A_{\tilde{t}}(\tau_{\tilde{t}})|^2, \quad (11)$$

where $A_t(\tau_t) = \frac{3}{2}\tau_t[1 + (1 - \tau_t)f(\tau_t)]$ (top quark loop) and $A_{\tilde{t}}$ (stop loop) are loop functions with $\tau_i = 4m_i^2/m_h^2$. The SM cross-section is $\sigma_{ggF}^{SM} \propto |A_t^{SM}|^2$, yielding the ratio,

$$\frac{\sigma_{SUSY}}{\sigma_{SM}} = \frac{\sigma_{ggF}}{\sigma_{ggF}^{SM}} = \left| \cos \theta + \frac{A_{\tilde{t}}}{A_t^{SM}} \right|^2 \sim 1. \quad (12)$$

For small mixing and large SUSY scale M_S , the production cross-section ratio approaches the Standard Model. Thus, deviations in the diphoton signal arise predominantly from the decay width [76],

$$\Gamma_{h \rightarrow \gamma\gamma} = \frac{\alpha^2 m_h^3}{1024\pi^3} \left| \frac{g_{hVV}}{m_V^2} Q_V^2 A_1(\tau_W) + \frac{2g_{h\bar{f}\bar{f}}}{m_f} N_{c,f} Q_f^2 A_{1/2}(\tau_f) + N_{c,S} Q_S^2 \frac{g_{hSS}}{m_S^2} A_0(\tau_S) \right|^2. \quad (13)$$

with loop amplitudes:

- $A_1(\tau_W)$ is the loop function of W -boson.

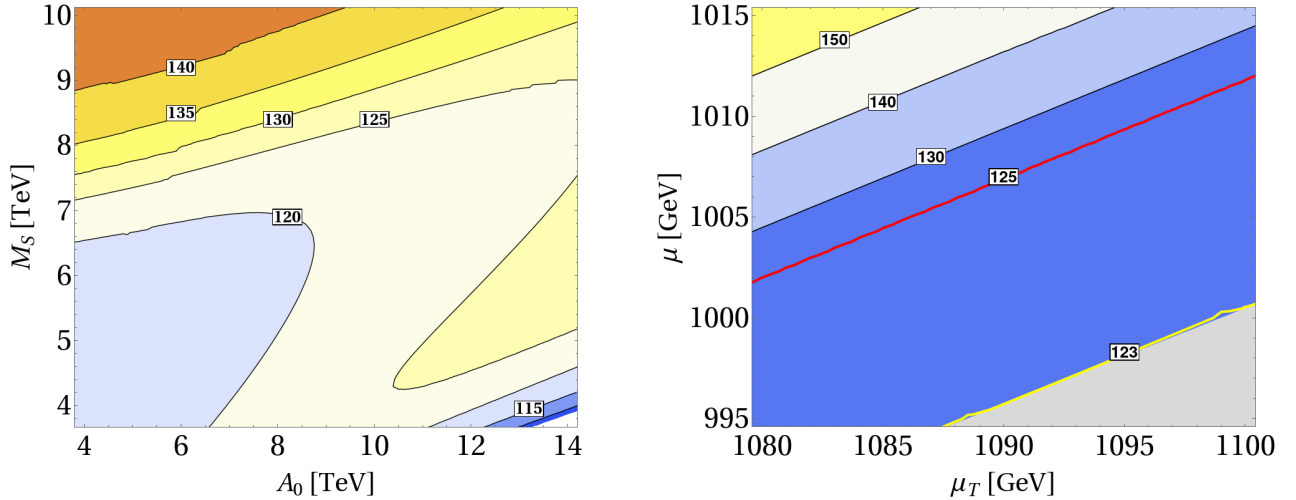


Figure 2. Left: Contour plot of the SM Higgs mass m_H in the A_0 - M_S parameter space, with $\mu = 1$ TeV, $\mu_T = 1.092$ TeV, and $B_{\mu_T} = 5$ (TeV) 2 . Right: Contour plot of the SM Higgs boson mass m_H in the μ - μ_T parameter space, with $M_S = 5.01$ TeV, $A_0 = 12$ TeV, and $B_{\mu_T} = 5$ (TeV) 2 .

- $A_0(\tau_s) = -\tau_i^2 [\tau_s^{-1} - f(\tau_s^{-1})]$ is the loop function of triplet charged Higgs.
- $A_{1/2}(\tau_f)$ is the loop function of chargino loop.

They reveal that additional contributions from charged Higgs bosons and charginos modify the Higgs decay width. For charginos, although heavier masses would naively induce larger deviations, their contribution is suppressed by the loop function $A_{1/2}(\tau_{\chi^\pm})$. This interplay naturally prevents unphysical growth of deviations while maintaining consistency with the decoupling theorem. Thus, the dominant contribution arises from the lightest charged Higgs boson (charged triplet) and moderate chargino mass, as numerically verified in Section IV.

III. NEUTRALINO SECTOR: RELIC DENSITY AND DIRECT DETECTION

The neutralino mass matrix includes the traditional neutralino components: the Bino ($\lambda_{\tilde{B}}$), Wino (\tilde{W}^0), and Higgsinos (\tilde{H}_d^0 , \tilde{H}_u^0), as well as the newly introduced fermionic triplet component, the triplino (λ_{T^0}). The specific form of the mass matrix is given as follows,

$$\begin{pmatrix} M_1 & 0 & -\frac{1}{2}g_1 v_d & \frac{1}{2}g_1 v_u & 0 \\ 0 & M_2 & \frac{1}{2}g_2 v_d & -\frac{1}{2}g_2 v_u & 0 \\ -\frac{1}{2}g_1 v_d & -\frac{1}{2}g_2 v_d & 0 & -\frac{1}{2}v_T \lambda - \mu & -\frac{1}{2}v_u \lambda \\ \frac{1}{2}g_1 v_u & -\frac{1}{2}g_2 v_u & -\frac{1}{2}v_T \lambda - \mu & 0 & -\frac{1}{2}v_d \lambda \\ 0 & 0 & -\frac{1}{2}v_u \lambda & -\frac{1}{2}v_d \lambda & 2\mu_T \end{pmatrix}. \quad (14)$$

To investigate the influence of various components on the DM annihilation process, the diagonal process can be employed to study the contribution of the triplino to DM in the

TMSSM. First, it is essential to diagonalize the neutralino mass matrix to derive its eigenvalue mass matrix,

$$N^* m_{\tilde{\chi}_0} N^\dagger = m_{\tilde{\chi}_0}^{\text{dia}}. \quad (15)$$

The contributions based on the components in the neutralino basis can be expressed as,

$$\begin{aligned} \lambda_{\tilde{B}} &= \sum_j N_{j1}^* \lambda_j^0, & \tilde{W}^0 &= \sum_j N_{j2}^* \lambda_j^0, & \tilde{H}_d^0 &= \sum_j N_{j3}^* \lambda_j^0, \\ \tilde{H}_u^0 &= \sum_j N_{j4}^* \lambda_j^0, & \lambda_{T^0} &= \sum_j N_{j5}^* \lambda_j^0. \end{aligned} \quad (16)$$

We select two benchmark points to examine their contributions to dark matter (DM) composition, as presented in Table I. These points represent Bino-dominated and Triplino-dominated DM scenarios. We exclude explicit discussion of the well-known Higgsino and Wino LSP scenarios.

In the parameter selection for ID A, the values are set as follows: $M_1 = 62.5$ GeV $\ll M_2, \mu, \mu_T$, and $\lambda = -0.1$. Specifically, the choice of M_1 aligns the bino mass precisely with the Higgs resonance region, significantly enhancing the annihilation efficiency via s -channel Higgs exchange.

In Fig. 3, the blue curve depicts the neutralino relic density, and the orange line indicates the observed dark matter relic density, $\Omega h^2 = 0.12$. The green dashed line shows the lightest neutralino mass, which increases linearly with M_1 , confirming its dominant bino composition. The bino relic density typically exceeds $\Omega h^2 = 0.12$, but two resonant regimes—where $2m_{\tilde{B}} \approx m_h$ or $2m_{\tilde{B}} \approx m_H$ —enable resonant annihilation, sharply reducing the relic density. Additionally, when the cyan dashed line (chargino mass) nears the bino mass, co-annihilation processes further decrease the relic density.

Therefore, analyzing the neutralino mixing matrix Z_N alone is insufficient to fully characterize the triplet sector's

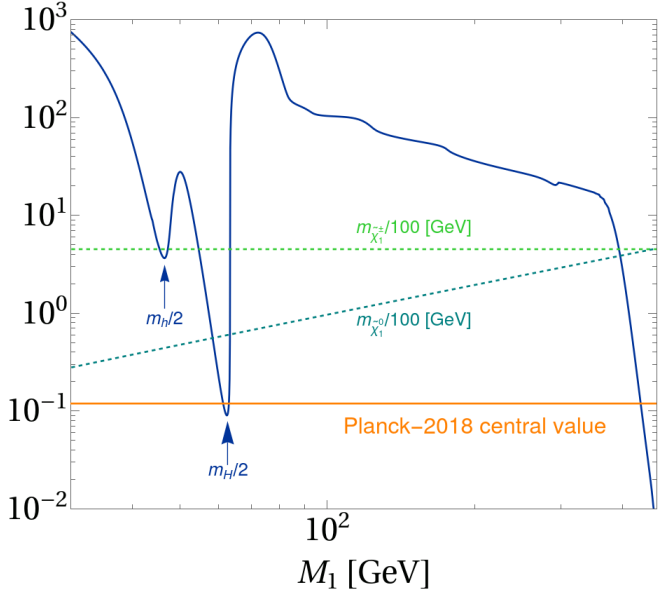


Figure 3. The blue solid line is the neutralino relic density with the variation of M_1 . The orange solid line is used to highlight the central relic density value from the Planck 2018 data. The green dashed line and cyan dashed line correspond to lightest chargino and lightest neutralino mass respectively. The input parameters are set as follows: $\tan\beta = 3.95$, $M_S = 5 \text{ TeV}$, $\lambda = -0.133$, $\mu_T = 200 \text{ GeV}$, $\mu = 1 \text{ TeV}$, $B_{\mu_T} = 5 (\text{TeV})^2$.

role in DM physics. As evidenced in Fig. 3, Bino–Chargino co-annihilation processes significantly enhance the DM annihilation cross-section [77–80]. A complete analysis therefore requires inclusion of the chargino mass matrix, defined in the basis $(\tilde{W}^-, \tilde{H}_d^-, \lambda_{T^-})$ and $(\tilde{W}^+, \tilde{H}_u^+, \lambda_{T^+})$. The chargino mass matrix is,

$$m_{\tilde{\chi}^\pm} = \begin{pmatrix} M_2 & \frac{1}{\sqrt{2}}g_2v_u & -g_2v_T \\ \frac{1}{\sqrt{2}}g_2v_d & -\frac{1}{2}v_T\lambda + \mu & -\frac{1}{\sqrt{2}}v_u\lambda \\ g_2v_T & \frac{1}{\sqrt{2}}v_d\lambda & 2\mu_T \end{pmatrix}. \quad (17)$$

In the limit of small λ and v_T , the mass matrix becomes nearly diagonal, showing that μ_T governs the charged triplino mass. This parameter also controls the masses of the lightest Higgs boson and triplino, allowing simultaneous study of Higgs and dark matter phenomenology through μ_T .

For the bino annihilation, the dominant process in the Higgs resonance region is bino pairs annihilating into bottom quarks via s -channel exchange of the Higgs boson [81]. This is natural, as the third-generation Yukawa coupling is the most significant. Additionally, Bino–Chargino co-annihilation processes happens naturally when $\mu_T \approx M_1$, with the dominant channels being $\tilde{\chi}_1^0 + \tilde{\chi}_1^\pm \rightarrow Z + W^-$ and $\tilde{\chi}_3^0 + \tilde{\chi}_1^\pm \rightarrow Z + W^-$.

In parameter set ID B, we set $\mu_T = 50 \text{ GeV}$ with $\mu_T \ll M_1, M_2, \mu$, ensuring the triplino is the LSP. However, the relic density is low, approximately 10^{-4} , due to strong SU(2) interactions similar to those of the wino, which requires a

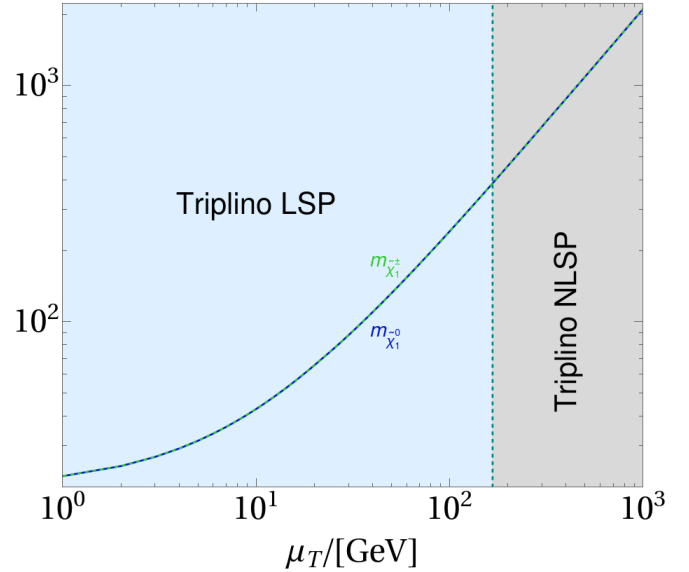


Figure 4. The masses of the charged triplino and neutral triplino as a function of μ_T , and the status for the LSP.

mass of $\sim 2 \text{ TeV}$ to match the observed relic density. Although a heavy triplino LSP appears viable for dark matter, Fig. 4 shows that the triplino ceases to be the LSP above $\sim 100 \text{ GeV}$. At tree level, with $\mu \gg M_1, M_2$, the neutral and charged triplinos are nearly degenerate ($m \approx 2\mu_T$) and dominate the LSP, as shown in Fig. 4. As μ_T increases, loop corrections raise the neutral triplino's mass more than the charged triplino's, because the neutral triplino, a Majorana fermion, experiences larger Z -boson and scalar loop effects, while the charged triplino, a Dirac fermion, incurs smaller photon and W -boson corrections. This inverts the mass hierarchy, making the charged triplino the LSP. Consequently, we adopt a bino LSP for this study.

We now consider the direct detection of neutralino dark matter [82], with a dominant bino component as established [83]. The spin-independent scattering cross-section between the neutralino and a nucleus originates from the effective Lagrangian [84],

$$\mathcal{L}_{\text{eff}} = a_q \bar{\chi}_1^0 \chi_1^0 \bar{q} q, \quad (18)$$

where a_q parametrizes the neutralino-quark coupling, and the resulting neutralino-nucleon cross-section becomes

$$\sigma_{\text{SI}} = \frac{4\mu_r^2}{\pi} \left(\sum_{q=u,d,s} f_{Tq}^{(p,n)} a_q \frac{m_{p,n}}{m_q} + \frac{2}{27} f_{TG}^{(p,n)} \sum_{q=c,b,t} a_q \frac{m_{p,n}}{m_q} \right)^2, \quad (19)$$

with μ_r the neutralino-nucleon reduced mass and $f_{TG}^{(p,n)} = 1 - \sum_{q=u,d,s} f_{Tq}^{(p,n)}$ and form factors are $f_{Tu}^{(p)} = 0.020 \pm 0.004$, $f_{Td}^{(p)} = 0.026 \pm 0.005$, $f_{Ts}^{(p)} = 0.118 \pm 0.062$, $f_{Tu}^{(n)} = 0.014 \pm 0.003$, $f_{Td}^{(n)} = 0.036 \pm 0.008$, $f_{Ts}^{(n)} = 0.118 \pm 0.062$ [85]. The dominant contribution to a_q/m_q stems from t -channel CP-

Z^N and Z^H Matrices					
ID A	$Z^N(1,1)$ -9.9918×10^{-1}	$Z^N(1,2)$ 5.1812×10^{-4}	$Z^N(1,3)$ -3.8790×10^{-2}	$Z^N(1,4)$ 1.1637×10^{-2}	Ωh^2 0.115
	$Z^N(1,5)$ 1.6007×10^{-4}	$Z^H(1,1)$ 3.4175×10^{-3}	$Z^H(1,2)$ 6.0784×10^{-2}	$Z^H(1,3)$ 9.9815×10^{-1}	
ID B	$Z^N(1,1)$ -2.0387×10^{-4}	$Z^N(1,2)$ 4.7161×10^{-4}	$Z^N(1,3)$ -2.2499×10^{-2}	$Z^N(1,4)$ 1.3659×10^{-2}	Ωh^2 5.8860×10^{-4}
	$Z^N(1,5)$ 9.9991×10^{-1}	$Z^H(1,1)$ 1.3531×10^{-2}	$Z^H(1,2)$ 6.5181×10^{-2}	$Z^H(1,3)$ 9.9778×10^{-1}	

Table I. Composition of Bino LSP and Triplino as Dark Matter and their Z^H .

even Higgs exchange, scaling as

$$\frac{a_q}{m_q} \simeq \sum_i \frac{S_{\chi\chi h_i}}{m_{h_i}^2} S_{h_i q q}. \quad (20)$$

For the lightest Higgs with mass $m_h \simeq 95.4$ GeV, the coupling is

$$S_{\chi\chi h_1} \simeq g_2(Z_{12}^N - \tan \theta_W Z_{11}^N)(Z_{11}^H Z_{13}^N - Z_{12}^H Z_{14}^N) + \lambda(Z_{11}^H Z_{15}^N Z_{13}^N + Z_{12}^H Z_{15}^N Z_{14}^N + Z_{13}^H Z_{13}^N Z_{14}^N) \quad (21)$$

where Z_{ij}^N , Z_{ij}^H , and λ denote neutralino mixing, Higgs mixing, and model parameters, respectively. Therefore, we obtain the cross section for ID A as 1.0110×10^{-11} pb, and for ID B as 6.3827×10^{-15} pb.

IV. NUMERICAL RESULT

We constructed the model's Lagrangian using SARAH v4.15.3 [86] and calculated the particle spectrum, including Higgs-mass loop corrections and diphoton signal strengths, with SPheno v4.0.5 [87, 88]. Theoretical consistency and experimental Higgs constraints were enforced via HiggsTools [89], HiggsBounds-5 [90–96], and HiggsSignals-2 [97–100], while the DM relic density and DM-nucleon cross-sections were computed with MicrOmegas v6.1.15 [101–106]. Collider limits were validated through SModelS v3 [107], and the entire workflow was automated using BSMArt v1.5 [108–117]. Fixed parameters are specified and Bayesian parameter estimation is performed using the MultiNest v3.12 [118–120] scanning the free parameter ranges given in Table II.

Before presenting our results, we define the conditions for the final selected parameter points. To address Higgs mass uncertainties from loop corrections, we set the lightest Higgs boson mass range as 94.4 GeV $\leq m_h \leq 96.4$ GeV, with the Standard Model Higgs boson mass at 123 GeV $\leq m_H \leq 127$ GeV. For Higgs data fitting, we incorporate direct search results for additional Higgs bosons from LEP, Tevatron, and LHC experiments. Selected parameter points must satisfy $\text{result} = 1$ in HiggsBounds with the HiggsSignal p -value

Fixed Parameters			
M_S/TeV	5	$\tan \beta$	3.95
A_0/TeV	12	M_2/TeV	1.5
M_3/TeV	3	A_λ/TeV	2
B_{μ_T}/TeV^2	5	B_μ/TeV^2	1
Scanned Parameter Ranges			
M_1/GeV	(45, 1200)	λ	(−0.3, 0.3)
μ_T/GeV	(500, 2000)	μ/GeV	(500, 2000)

Table II. Parameter space of the TMSSM: Fixed values (top) and scanned ranges (bottom).

obtained via χ^2 analysis exceeding 0.05 to ensure statistical significance and experimental consistency.

To account for the systematic uncertainties in DM calculations, we adopt an expanded relic density range of $\Omega h^2 \in [0.096, 0.144]$, corresponding to $\pm 20\%$ variations around the Planck-2018 observed cold DM central value $\Omega h^2 = 0.120$ [121]. For direct and indirect detection constraints, we require a DM signal exclusion statistical reliability of $p \geq 0.05$ at the 95% confidence level, while collider limits are enforced via the SModelS exclusion ratio criterion $r < 1$ [107].

We additionally require a lower bound $m_{H^\pm} > 110$ GeV on the charged Higgs mass from stau ($\tilde{\tau}$) searches, following the analysis of Ref. [64]. The similar final-state signatures between $\tilde{\tau}^\pm \rightarrow \tau^\pm \tilde{\chi}_1^0$ and $H^\pm \rightarrow \tau \nu$ decays (for massless neutrinos) allow reinterpretation of ATLAS stau search results. The current exclusion limits rule out charged triplet scalars below 110 GeV.

The color scheme employed in the scatter plot adheres to the following consistent convention:

- Red points:

$$\begin{aligned} m_H &= 125 \pm 2 \text{ GeV}, & \text{HBresult} &= 1, \\ \text{HSpval} &\geq 0.05, & \Omega h^2 &= 0.120 \pm 0.024, \\ \text{DMpval} &\geq 0.05, & \text{SModelSr} &< 1, \\ \mu_{\gamma\gamma} &= 0.24^{+0.09}_{-0.08}, & m_H^\pm &\geq 110 \text{ GeV} \end{aligned} \quad (22)$$

- Cyan points (Higgs constraints): SM Higgs mass lies

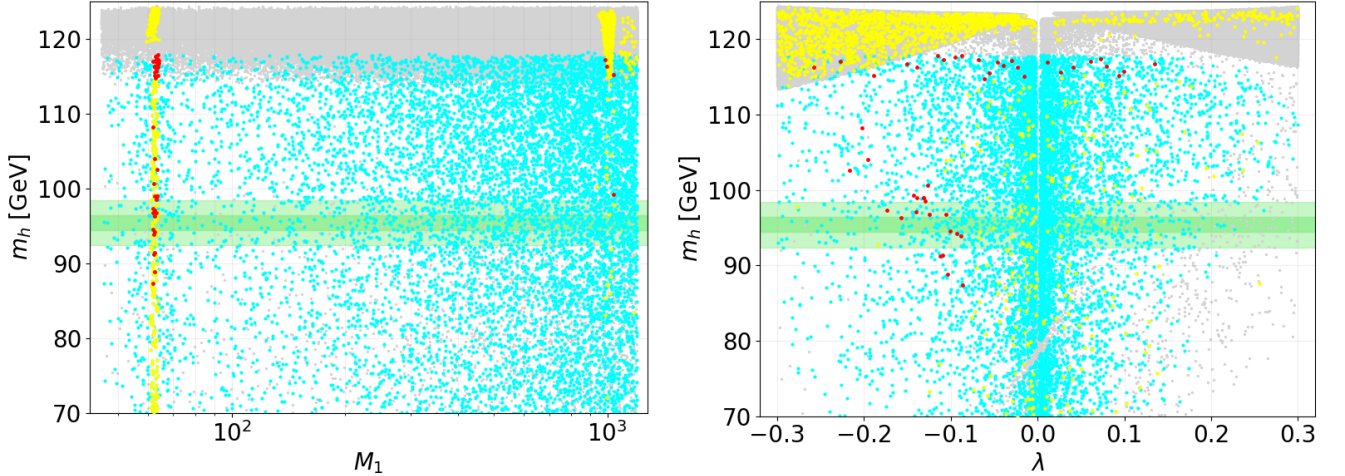


Figure 5. The scanning results using the parameter ranges in Table II are shown. The left panel displays the relationship between the light scalar Higgs boson mass m_h and M_1 , while the right panel presents the correlation between m_h and λ . The color scheme follows the description in Eq 22 and the surrounding context. The green band indicates that $m_h = 95.4 \pm 1$ GeV, the light green area represents $m_h = 95.4 \pm 3$ GeV.

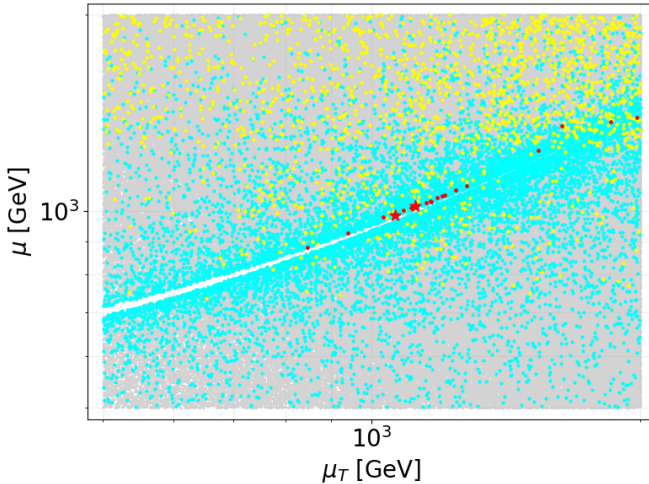


Figure 6. The results of the global scan are presented in the $\mu - \mu_T$ plane. The color coding of the parameter points follows Equation 22 and the text below it. The red star points are based on the red points, with the additional condition of $m_h = 95.4 \pm 1$ GeV.

within the experimentally allowed range and satisfies all constraints from HB, HS, and SModelS.

- Yellow points (DM constraints): Ωh^2 lies within a $\pm 20\%$ range, DM p-value satisfies statistical requirements and $SModelSr < 1$.
- Gray points: Only $SModelSr < 1$.

The left panel of Fig. 5 shows that the cyan data points are nearly independent of M_1 . This is because M_1 only affects the bino mass, which plays no role in the Higgs sector. In contrast, the yellow data points display a specific distri-

bution, where the first cluster lies in the Higgs resonance region at $M_1 \approx m_H/2$. The second cluster appears near the TeV energy scale. This pattern matches our earlier findings reported in Fig. 3. In the low-energy Higgs resonance region, the bino mass M_1 is much smaller than the higgsino mass μ and the triplino mass $2\mu_T$. This enables the region to yield a pure bino dark matter candidate consistent with observational constraints. At the TeV scale, the near degeneracy of $M_1 \sim \mu \sim \mu_T$ facilitates bino-higgsino or bino-triplino coannihilation via gauge-mediated interactions. This configuration boosts the efficiency of annihilation, yielding a correct DM relic density. Diphoton excess further reduces the yellow points to fewer red points. Then we can find the overall constraint still has survival points touching the correct 95 GeV Higgs band.

In the right panel of Fig. 5, the quartic coupling λ exhibits a Z_2 symmetry $\lambda \rightarrow -\lambda$ because it enters the Higgs and DM observables only through λ^2 . Most points satisfying the Higgs constraints have $m_h > 110$ GeV. The yellow points are predominantly in the negative λ region due to the collective influence of parameters such as M_1 , μ , and μ_T , rather than a direct effect of λ itself. As λ decreases, the density of points with $m_h < 110$ GeV increases, reflecting the interplay of λ , μ , and μ_T in the expression for m_h (Eq.8). Notably, some red points lie within the theoretically predicted green band to match the 95 GeV Higgs requirement.

Finally, in Fig. 6, the cyan points satisfying the Higgs constraints are diffusely distributed, showing no significant correlation with μ or μ_T . This indicates that the Higgs constraints impose relatively weak limits on these mass parameters. The yellow points, which satisfy the dark matter constraints, depend on the higgsino mass parameter μ , with their density increasing as μ increases. This occurs because the bino can become the LSP and achieve the correct relic density only for larger μ . The red points, indicating constraints on the light scalar Higgs boson mass m_h and signal strength, show a linear

dependence on μ and μ_T . This narrow band results from the cancellation between these mass parameters, consistent with Fig.1 and Eq.8. The jagged white regions represent parameter space where the triplino is the next-to-lightest stable particle, consistent with Fig.4.

V. CONCLUSIONS

This study systematically explores the TMSSM to explain the 95 GeV Higgs boson diphoton excess observed by CMS and ATLAS and its implications for DM physics. By incorporating an $SU(2)_L$ triplet superfield, TMSSM reduces fine-tuning issues of the MSSM and naturally supports Higgs boson masses at 95 GeV and 125 GeV. Our calculations show that optimizing triplet-doublet mixing and parameters λ and μ_T enables TMSSM to reproduce the experimental diphoton signal strength, $\mu_{\gamma\gamma}^{\text{CMS+ATLAS}} = 0.24^{+0.09}_{-0.08}$. In the DM sector, the triplet and its supersymmetric partner, the triplino, enhance neutralino annihilation through Higgs resonance and co-annihilation, achieving consistency with the Planck-2018 cold DM relic density, $\Omega h^2 = 0.120 \pm 0.024$, while meeting

direct and indirect detection constraints.

Using tools like SARAH, SPheno, MicrOmegas, and BS-MArts, we performed a comprehensive scan of the TMSSM parameter space, identifying regions that simultaneously satisfy Higgs masses, $m_h \approx 95.4 \pm 1$ GeV and $m_H \approx 125 \pm 2$ GeV, diphoton signal strength, and DM relic density requirements. These findings confirm that TMSSM robustly explains the 95 GeV diphoton excess and provides a consistent framework for DM physics. Future collider experiments, such as the High-Luminosity LHC or a next-generation circular collider, will precisely probe triplino properties and the 95 GeV Higgs signal, offering critical tests of TMSSM and deeper insights into supersymmetric physics.

ACKNOWLEDGMENTS

We thank Mark Goodsell and Andreas Crivellin for the helpful discussions. This work is supported by the National Natural Science Foundation of China (NNSFC) under grant Nos. 12275232, No. 12335005.

-
- [1] L. Randall and R. Sundrum, *Phys. Rev. Lett.* **83**, 3370 (1999), [arXiv:hep-ph/9905221](#).
 - [2] N. Arkani-Hamed, S. Dimopoulos, and G. R. Dvali, *Phys. Lett. B* **429**, 263 (1998), [arXiv:hep-ph/9803315](#).
 - [3] H. E. Haber and G. L. Kane, *Phys. Rept.* **117**, 75 (1985).
 - [4] S. P. Martin, *Adv. Ser. Direct. High Energy Phys.* **18**, 1 (1998), [arXiv:hep-ph/9709356](#).
 - [5] G. Jungman, M. Kamionkowski, and K. Griest, *Phys. Rept.* **267**, 195 (1996), [arXiv:hep-ph/9506380](#).
 - [6] G. H. Duan, W. Wang, L. Wu, J. M. Yang, and J. Zhao, *Phys. Lett. B* **778**, 296 (2018), [arXiv:1711.03893](#) [hep-ph].
 - [7] R. Kitano and Y. Nomura, *Phys. Rev. D* **73**, 095004 (2006), [arXiv:hep-ph/0602096](#).
 - [8] M. Papucci, J. T. Ruderman, and A. Weiler, *JHEP* **09**, 035 (2012), [arXiv:1110.6926](#) [hep-ph].
 - [9] A. Strumia, *JHEP* **04**, 073 (2011), [arXiv:1101.2195](#) [hep-ph].
 - [10] N. Craig, A. Katz, M. Strassler, and R. Sundrum, *JHEP* **07**, 105 (2015), [arXiv:1501.05310](#) [hep-ph].
 - [11] A. Hayrapetyan *et al.* (CMS), *Phys. Rev. D* **109**, 072007 (2024), [arXiv:2309.16823](#) [hep-ex].
 - [12] G. Aad *et al.* (ATLAS), *Phys. Rept.* **1116**, 261 (2025), [arXiv:2403.02455](#) [hep-ex].
 - [13] J. R. Espinosa and M. Quiros, *Nucl. Phys. B* **384**, 113 (1992).
 - [14] S. Di Chiara and K. Hsieh, *Phys. Rev. D* **78**, 055016 (2008), [arXiv:0805.2623](#) [hep-ph].
 - [15] T. Basak and S. Mohanty, *Phys. Rev. D* **86**, 075031 (2012), [arXiv:1204.6592](#) [hep-ph].
 - [16] L. Cort, M. Garcia, and M. Quiros, *Phys. Rev. D* **88**, 075010 (2013), [arXiv:1308.4025](#) [hep-ph].
 - [17] P. Bandyopadhyay, K. Huitu, and A. Sabanci, *JHEP* **10**, 091 (2013), [arXiv:1306.4530](#) [hep-ph].
 - [18] P. Bandyopadhyay, S. Di Chiara, K. Huitu, and A. S. Keçeli, *JHEP* **11**, 062 (2014), [arXiv:1407.4836](#) [hep-ph].
 - [19] M. Garcia-Pepin, S. Gori, M. Quiros, R. Vega, R. Vega-Morales, and T.-T. Yu, *Phys. Rev. D* **91**, 015016 (2015), [arXiv:1409.5737](#) [hep-ph].
 - [20] P. Bandyopadhyay, C. Coriano, and A. Costantini, *JHEP* **09**, 045 (2015), [arXiv:1506.03634](#) [hep-ph].
 - [21] P. Bandyopadhyay, C. Corianò, and A. Costantini, *Phys. Rev. D* **94**, 055030 (2016), [arXiv:1512.08651](#) [hep-ph].
 - [22] P. Bandyopadhyay, C. Coriano, and A. Costantini, *JHEP* **12**, 127 (2015), [arXiv:1510.06309](#) [hep-ph].
 - [23] J. L. Diaz-Cruz, J. Hernandez-Sánchez, S. Moretti, and A. Rosado, *Phys. Rev. D* **77**, 035007 (2008), [arXiv:0710.4169](#) [hep-ph].
 - [24] C. Arina, V. Martin-Lozano, and G. Nardini, *JHEP* **08**, 015 (2014), [arXiv:1403.6434](#) [hep-ph].
 - [25] E. Barradas-Guevara, O. Felix-Beltran, and A. Rosado, *Phys. Rev. D* **71**, 073004 (2005), [arXiv:hep-ph/0408196](#).
 - [26] M. Das, S. Di Chiara, and S. Roy, *Phys. Rev. D* **91**, 055013 (2015), [arXiv:1501.02667](#) [hep-ph].
 - [27] P. Fileviez Perez and M. B. Wise, *Phys. Rev. D* **84**, 055015 (2011), [arXiv:1105.3190](#) [hep-ph].
 - [28] A. M. Sirunyan *et al.* (CMS), *Phys. Lett. B* **793**, 320 (2019), [arXiv:1811.08459](#) [hep-ex].
 - [29] CMS collaboration (CMS), CMS-PAS-HIG-20-002 (2018), Search for a standard model-like Higgs boson in the mass range between 70 and 110 GeV in the diphoton final state in proton-proton collisions at $\sqrt{s} = 13$ TeV.
 - [30] ATLAS collaboration (ATLAS), ATLAS-CONF-2018-025 (2018), Search for resonances in the 65 to 110 GeV diphoton invariant mass range using 80 fb^{-1} of pp collisions collected at $\sqrt{s} = 13$ TeV with the ATLAS detector.
 - [31] ATLAS collaboration (ATLAS), ATLAS-CONF-2023-035 (2023), Search for diphoton resonances in the 66 to 110 GeV mass range using 140 fb^{-1} of 13 TeV pp collisions collected with the ATLAS detector.
 - [32] T. Biekötter, S. Heinemeyer, and G. Weiglein, *Phys. Rev. D* **109**, 035005 (2024), [arXiv:2306.03889](#) [hep-ph].
 - [33] J. Cao, X. Guo, Y. He, P. Wu, and Y. Zhang, *Phys. Rev. D* **95**,

- 116001 (2017), arXiv:1612.08522 [hep-ph].
- [34] A. Crivellin, J. Heeck, and D. Müller, *Phys. Rev. D* **97**, 035008 (2018), arXiv:1710.04663 [hep-ph].
- [35] U. Haisch and A. Malinauskas, *JHEP* **03**, 135 (2018), arXiv:1712.06599 [hep-ph].
- [36] P. J. Fox and N. Weiner, *JHEP* **08**, 025 (2018), arXiv:1710.07649 [hep-ph].
- [37] D. Liu, J. Liu, C. E. M. Wagner, and X.-P. Wang, *JHEP* **06**, 150 (2018), arXiv:1805.01476 [hep-ph].
- [38] K. Wang, F. Wang, J. Zhu, and Q. Jie, *Chin. Phys. C* **42**, 103109 (2018), arXiv:1811.04435 [hep-ph].
- [39] L. Liu, H. Qiao, K. Wang, and J. Zhu, *Chin. Phys. C* **43**, 023104 (2019), arXiv:1812.00107 [hep-ph].
- [40] T. Biekötter, M. Chakraborti, and S. Heinemeyer, *Eur. Phys. J. C* **80**, 2 (2020), arXiv:1903.11661 [hep-ph].
- [41] J. M. Cline and T. Toma, *Phys. Rev. D* **100**, 035023 (2019), arXiv:1906.02175 [hep-ph].
- [42] K. Choi, S. H. Im, K. S. Jeong, and C. B. Park, *Eur. Phys. J. C* **79**, 956 (2019), arXiv:1906.03389 [hep-ph].
- [43] A. Kundu, S. Maharana, and P. Mondal, *Nucl. Phys. B* **955**, 115057 (2020), arXiv:1907.12808 [hep-ph].
- [44] J. Cao, X. Jia, Y. Yue, H. Zhou, and P. Zhu, *Phys. Rev. D* **101**, 055008 (2020), arXiv:1908.07206 [hep-ph].
- [45] T. Biekötter, M. Chakraborti, and S. Heinemeyer, *Int. J. Mod. Phys. A* **36**, 2142018 (2021), arXiv:2003.05422 [hep-ph].
- [46] A. A. Abdelalim, B. Das, S. Khalil, and S. Moretti, *Nucl. Phys. B* **985**, 116013 (2022), arXiv:2012.04952 [hep-ph].
- [47] S. Heinemeyer, C. Li, F. Lika, G. Moortgat-Pick, and S. Paasch, *Phys. Rev. D* **106**, 075003 (2022), arXiv:2112.11958 [hep-ph].
- [48] T. Biekötter, S. Heinemeyer, and G. Weiglein, *JHEP* **08**, 201 (2022), arXiv:2203.13180 [hep-ph].
- [49] S. Iguro, T. Kitahara, and Y. Omura, *Eur. Phys. J. C* **82**, 1053 (2022), arXiv:2205.03187 [hep-ph].
- [50] W. Li, J. Zhu, K. Wang, S. Ma, P. Tian, and H. Qiao, (2022), arXiv:2212.11739 [hep-ph].
- [51] T. Biekötter, S. Heinemeyer, and G. Weiglein, (2023), arXiv:2303.12018 [hep-ph].
- [52] C. Bonilla, A. E. Carcamo Hernandez, S. Kovalenko, H. Lee, R. Pasechnik, and I. Schmidt, (2023), arXiv:2305.11967 [hep-ph].
- [53] D. Azevedo, T. Biekötter, and P. M. Ferreira, (2023), arXiv:2305.19716 [hep-ph].
- [54] P. Escribano, V. M. Lozano, and A. Vicente, (2023), arXiv:2306.03735 [hep-ph].
- [55] A. Belyaev, R. Benbrik, M. Boukidi, M. Chakraborti, S. Moretti, and S. Semlali, (2023), arXiv:2306.09029 [hep-ph].
- [56] S. Ashanujjaman, S. Banik, G. Coloretti, A. Crivellin, B. Mellado, and A.-T. Mulaudzi, *Phys. Rev. D* **108**, L091704 (2023), arXiv:2306.15722 [hep-ph].
- [57] S. Baek, P. Ko, Y. Omura, and C. Yu, (2024), arXiv:2412.02178 [hep-ph].
- [58] X. Du, H. Liu, and Q. Chang, (2025), arXiv:2502.06444 [hep-ph].
- [59] S. Yaser Ayazi, M. Hosseini, S. Paktnat Mehdiabadi, and R. Rouzbehi, *Phys. Rev. D* **110**, 055004 (2024), arXiv:2405.01132 [hep-ph].
- [60] D. Borah, S. Mahapatra, P. K. Paul, and N. Sahu, *Phys. Rev. D* **109**, 055021 (2024), arXiv:2310.11953 [hep-ph].
- [61] S. Bhattacharya, G. Coloretti, A. Crivellin, S.-E. Dahbi, Y. Fang, M. Kumar, and B. Mellado, (2023), arXiv:2306.17209 [hep-ph].
- [62] G. Coloretti, A. Crivellin, and B. Mellado, *Phys. Rev. D* **110**, 073001 (2024), arXiv:2312.17314 [hep-ph].
- [63] S. Banik, G. Coloretti, A. Crivellin, and B. Mellado, *JHEP* **01**, 155 (2025), arXiv:2308.07953 [hep-ph].
- [64] S. Ashanujjaman, S. Banik, G. Coloretti, A. Crivellin, S. P. Maharathy, and B. Mellado, *JHEP* **04**, 003 (2025), arXiv:2411.18618 [hep-ph].
- [65] P. S. B. Dev, R. N. Mohapatra, and Y. Zhang, *Phys. Lett. B* **849**, 138481 (2024), arXiv:2312.17733 [hep-ph].
- [66] T. Mondal, S. Moretti, and P. Sanyal, (2024), arXiv:2412.00474 [hep-ph].
- [67] J. Cao, X. Jia, J. Lian, and L. Meng, *Phys. Rev. D* **109**, 075001 (2024), arXiv:2310.08436 [hep-ph].
- [68] U. Ellwanger and C. Hugonie, *Eur. Phys. J. C* **83**, 1138 (2023), arXiv:2309.07838 [hep-ph].
- [69] J. Lian, *Phys. Rev. D* **110**, 115018 (2024), arXiv:2406.10969 [hep-ph].
- [70] U. Ellwanger, C. Hugonie, S. F. King, and S. Moretti, *Eur. Phys. J. C* **84**, 788 (2024), arXiv:2404.19338 [hep-ph].
- [71] U. Ellwanger and C. Hugonie, *Eur. Phys. J. C* **84**, 526 (2024), arXiv:2403.16884 [hep-ph].
- [72] J. Cao, X. Jia, and J. Lian, *Phys. Rev. D* **110**, 115039 (2024), arXiv:2402.15847 [hep-ph].
- [73] C.-X. Liu, Y. Zhou, X.-Y. Zheng, J. Ma, T.-F. Feng, and H.-B. Zhang, *Phys. Rev. D* **109**, 056001 (2024), arXiv:2402.00727 [hep-ph].
- [74] J. Edsjo and P. Gondolo, *Phys. Rev. D* **56**, 1879 (1997), arXiv:hep-ph/9704361.
- [75] A. Delgado, M. Garcia-Pepin, B. Ostdiek, and M. Quiros, *Phys. Rev. D* **92**, 015011 (2015), arXiv:1504.02486 [hep-ph].
- [76] A. Djouadi, *Phys. Rept.* **459**, 1 (2008), arXiv:hep-ph/0503173.
- [77] M. Abdughani, L. Wu, and J. M. Yang, *Eur. Phys. J. C* **78**, 4 (2018), arXiv:1705.09164 [hep-ph].
- [78] G. H. Duan, K.-I. Hikasa, J. Ren, L. Wu, and J. M. Yang, *Phys. Rev. D* **98**, 015010 (2018), arXiv:1804.05238 [hep-ph].
- [79] M. Abdughani and L. Wu, *Eur. Phys. J. C* **80**, 233 (2020), arXiv:1908.11350 [hep-ph].
- [80] G. H. Duan, C. Han, B. Peng, L. Wu, and J. M. Yang, *Phys. Lett. B* **788**, 475 (2019), arXiv:1809.10061 [hep-ph].
- [81] N. Arkani-Hamed, A. Delgado, and G. F. Giudice, *Nucl. Phys. B* **741**, 108 (2006), arXiv:hep-ph/0601041.
- [82] Z.-J. Yang, J.-L. Yang, S.-M. Zhao, X.-G. Wu, and T.-F. Feng, *Eur. Phys. J. C* **84**, 1216 (2024), arXiv:2410.13659 [hep-ph].
- [83] C. Cheung, L. J. Hall, D. Pinner, and J. T. Ruderman, *JHEP* **05**, 100 (2013), arXiv:1211.4873 [hep-ph].
- [84] T. Basak and S. Mohanty, *JHEP* **08**, 020 (2013), arXiv:1304.6856 [hep-ph].
- [85] J. R. Ellis, A. Ferstl, and K. A. Olive, *Phys. Lett. B* **481**, 304 (2000), arXiv:hep-ph/0001005.
- [86] F. Staub, (2008), arXiv:0806.0538 [hep-ph].
- [87] W. Porod, *Comput. Phys. Commun.* **153**, 275 (2003), arXiv:hep-ph/0301101.
- [88] W. Porod and F. Staub, *Comput. Phys. Commun.* **183**, 2458 (2012), arXiv:1104.1573 [hep-ph].
- [89] H. Bahl, T. Biekötter, S. Heinemeyer, C. Li, S. Paasch, G. Weiglein, and J. Wittbrodt, *Comput. Phys. Commun.* **291**, 108803 (2023), arXiv:2210.09332 [hep-ph].
- [90] P. Bechtle, O. Brein, S. Heinemeyer, G. Weiglein, and K. E. Williams, *Comput. Phys. Commun.* **181**, 138 (2010), arXiv:0811.4169 [hep-ph].
- [91] P. Bechtle, O. Brein, S. Heinemeyer, G. Weiglein, and K. E. Williams, *Comput. Phys. Commun.* **182**, 2605 (2011), arXiv:1102.1898 [hep-ph].
- [92] P. Bechtle, O. Brein, S. Heinemeyer, O. Stal, T. Stefaniak, G. Weiglein, and K. Williams, *PoS CHARGED2012*, 024

- (2012), arXiv:1301.2345 [hep-ph].
- [93] P. Bechtle, O. Brein, S. Heinemeyer, O. Stål, T. Stefaniak, G. Weiglein, and K. E. Williams, *Eur. Phys. J. C* **74**, 2693 (2014), arXiv:1311.0055 [hep-ph].
- [94] P. Bechtle, S. Heinemeyer, O. Stål, T. Stefaniak, and G. Weiglein, *Eur. Phys. J. C* **75**, 421 (2015), arXiv:1507.06706 [hep-ph].
- [95] P. Bechtle, D. Dercks, S. Heinemeyer, T. Klingl, T. Stefaniak, G. Weiglein, and J. Wittbrodt, *Eur. Phys. J. C* **80**, 1211 (2020), arXiv:2006.06007 [hep-ph].
- [96] H. Bahl, V. M. Lozano, T. Stefaniak, and J. Wittbrodt, *Eur. Phys. J. C* **82**, 584 (2022), arXiv:2109.10366 [hep-ph].
- [97] P. Bechtle, S. Heinemeyer, O. Stål, T. Stefaniak, and G. Weiglein, *Eur. Phys. J. C* **74**, 2711 (2014), arXiv:1305.1933 [hep-ph].
- [98] O. Stål and T. Stefaniak, PoS **EPS-HEP2013**, 314 (2013), arXiv:1310.4039 [hep-ph].
- [99] P. Bechtle, S. Heinemeyer, O. Stål, T. Stefaniak, and G. Weiglein, *JHEP* **11**, 039 (2014), arXiv:1403.1582 [hep-ph].
- [100] P. Bechtle, S. Heinemeyer, T. Klingl, T. Stefaniak, G. Weiglein, and J. Wittbrodt, *Eur. Phys. J. C* **81**, 145 (2021), arXiv:2012.09197 [hep-ph].
- [101] G. Belanger, F. Boudjema, A. Pukhov, and A. Semenov, *Comput. Phys. Commun.* **176**, 367 (2007), arXiv:hep-ph/0607059.
- [102] G. Belanger, F. Boudjema, A. Pukhov, and A. Semenov, *Comput. Phys. Commun.* **180**, 747 (2009), arXiv:0803.2360 [hep-ph].
- [103] G. Belanger, F. Boudjema, A. Pukhov, and A. Semenov, *Nuovo Cim. C* **033N2**, 111 (2010), arXiv:1005.4133 [hep-ph].
- [104] G. Belanger, F. Boudjema, A. Pukhov, and A. Semenov, *Comput. Phys. Commun.* **185**, 960 (2014), arXiv:1305.0237 [hep-ph].
- [105] G. Bélanger, F. Boudjema, A. Pukhov, and A. Semenov, *Comput. Phys. Commun.* **192**, 322 (2015), arXiv:1407.6129 [hep-ph].
- [106] G. Bélanger, F. Boudjema, A. Goudelis, A. Pukhov, and B. Zaldivar, *Comput. Phys. Commun.* **231**, 173 (2018), arXiv:1801.03509 [hep-ph].
- [107] M. M. Altakach, S. Kraml, A. Lessa, S. Narasimha, T. Pascal, C. Ramos, Y. Villamizar, and W. Waltenberger, (2024), arXiv:240x.nnnnn [hep-ph].
- [108] M. D. Goodsell and A. Joury, *Comput. Phys. Commun.* **297**, 109057 (2024), arXiv:2301.01154 [hep-ph].
- [109] A. E. Faraggi and M. D. Goodsell, *Eur. Phys. J. C* **84**, 589 (2024), arXiv:2312.13411 [hep-ph].
- [110] B. Fuks, M. D. Goodsell, and T. Murphy, *Phys. Rev. D* **111**, 055010 (2025), arXiv:2409.03014 [hep-ph].
- [111] D. Agin, B. Fuks, M. D. Goodsell, and T. Murphy, *Phys. Lett. B* **853**, 138597 (2024), arXiv:2311.17149 [hep-ph].
- [112] D. Agin, B. Fuks, M. D. Goodsell, and T. Murphy, *Eur. Phys. J. C* **84**, 1218 (2024), arXiv:2404.12423 [hep-ph].
- [113] K. Benakli, M. Goodsell, W. Ke, and P. Slavich, *Eur. Phys. J. C* **83**, 43 (2023), arXiv:2208.05867 [hep-ph].
- [114] M. D. Goodsell and A. Joury, *Eur. Phys. J. C* **83**, 268 (2023), arXiv:2204.13950 [hep-ph].
- [115] M. D. Goodsell and L. Priya, *Eur. Phys. J. C* **82**, 235 (2022), arXiv:2106.08815 [hep-ph].
- [116] M. D. Goodsell and R. Moutafis, *Eur. Phys. J. C* **81**, 808 (2021), arXiv:2012.09022 [hep-ph].
- [117] G. Domènech, M. Goodsell, and C. Wetterich, *JHEP* **01**, 180 (2021), arXiv:2008.04310 [hep-ph].
- [118] F. Feroz and M. P. Hobson, *Mon. Not. Roy. Astron. Soc.* **384**, 449 (2008), arXiv:0704.3704 [astro-ph].
- [119] F. Feroz, M. P. Hobson, and M. Bridges, *Mon. Not. Roy. Astron. Soc.* **398**, 1601 (2009), arXiv:0809.3437 [astro-ph].
- [120] F. Feroz, M. P. Hobson, E. Cameron, and A. N. Pettitt, *Open J. Astrophys.* **2**, 10 (2019), arXiv:1306.2144 [astro-ph.IM].
- [121] N. Aghanim *et al.* (Planck), *Astron. Astrophys.* **641**, A6 (2020), [Erratum: *Astron. Astrophys.* 652, C4 (2021)], arXiv:1807.06209 [astro-ph.CO].